



## Two different donor subunits substituted unsymmetrical squaraines for solution-processed small molecule organic solar cells



Daobin Yang<sup>a, b, 1</sup>, Yan Jiao<sup>a, 1</sup>, Yan Huang<sup>a, \*</sup>, Taojun Zhuang<sup>b</sup>, Lin Yang<sup>a</sup>, Zhiyun Lu<sup>a, \*\*</sup>, Xuemei Pu<sup>a</sup>, Hisahiro Sasabe<sup>b, \*\*\*</sup>, Junji Kido<sup>b, \*\*\*\*</sup>

<sup>a</sup> Key Laboratory of Green Chemistry and Technology (Ministry of Education), College of Chemistry, Sichuan University, Chengdu 610064, PR China

<sup>b</sup> Department of Organic Device Engineering, Research Center for Organic Electronics, Yamagata University, Yonezawa 992-8510, Japan

### ARTICLE INFO

#### Article history:

Received 6 January 2016  
Received in revised form  
4 February 2016  
Accepted 9 February 2016  
Available online xxx

#### Keywords:

Unsymmetrical squaraines  
Donor subunits  
H- and J-aggregation  
Solution-processed  
Small molecule organic solar cells

### ABSTRACT

Two unsymmetrical squaraines (USQs) with different donor (D) subunits as photovoltaic materials, namely USQ-11 and USQ-12, were designed and synthesized to investigate the effect of different D subunits on the optoelectronic properties of USQs for the first time. The two USQs compounds were characterized for optical, electrochemical, quantum chemical and optoelectronic properties. By changing the two different D subunits attached to the squaric acid core from 2,3,3-trimethylindolenine to 2-methylbenzothiazole, the HOMO energy levels could be tuned with a stepping of 0.07 eV, and quite different solid state aggregations (H- or J-aggregation) were observed in the thin film by UV-Vis absorption spectra, which were attributed to their distinct steric effects and dipole moments. Solution-processed bulk-heterojunction small molecule organic solar cells fabricated with the USQ-11/PC<sub>71</sub>BM (1:5, wt%) exhibited extremely higher PCE (4.27%) than that of the USQ-12/PC<sub>71</sub>BM (2.78%). The much enhanced PCE should be attributed to the simultaneously improved  $V_{oc}$ ,  $J_{sc}$  and FF.

© 2016 Elsevier B.V. All rights reserved.

### 1. Introduction

Solution-processed bulk-heterojunction (BHJ) organic solar cells (OSCs) based on small molecules (SM) have shown great potential as an alternative to more conventional polymer-based OSCs, because of their well-defined molecular structure, high purity and batch to batch reproducibility [1,2]. So far, the power conversion efficiency (PCE) of small molecule based OSCs already exceeded 10% [3], however further improved PCE is still needed for commercial application, thus much research effort has been devoted to the molecular tailoring of photovoltaic materials, so that the correlations between molecular structure and photovoltaic properties could be revealed.

Squaraines have drawn more and more attention in recent

years, since they possess extremely high molar extinction coefficients, intense and broad absorption in Vis-NIR spectral regions [4–9]. Generally, they can be divided into symmetrical squaraines (SQs) and unsymmetrical squaraines (USQs). In comparison with SQs, USQs bearing a D-A-D' rather than D-A-D molecular skeleton should be more promising due to their much higher structural tunability. At the beginning, the PCEs of the USQs-based BHJ-OSCs were unsatisfactory (0.16–2.05%), which should be ascribed to their low  $V_{oc}$  (0.24–0.69 V),  $J_{sc}$  (1.40–9.05 mA cm<sup>-2</sup>) and FF (0.27–0.45) [10–13]. Recently, a series of novel USQs materials for BHJ-SMOSCs have been developed by our group, in which 1,1,2-trimethyl-1H-benzo[e]indole was used as D subunit, and 2,6-dihydroxyphenyl groups were used as D' segments [14–17]. Through delicate molecular design mainly at the end-capping group of the D' segments, such as diisobutylamino, diarylamino, carbazyl, indoline and tetrahydroquinoline groups, the PCEs of these USQs-based BHJ-SMOSCs increased from 1.54% to 4.29%, which were attributed to their high  $V_{oc}$  (0.75–1.12 V),  $J_{sc}$  (5.40–11.03 mA cm<sup>-2</sup>) and FF (0.36–0.48). So far, the PCEs of solution-processed USQs-based BHJ-SMOSCs have reached 6.00% [18,19], which were higher than that of the classic SQs materials (PCE = 5.50%) [20]. These encouraging results indicated that indoline unit could acts as a quite promising end-capping unit to

\* Corresponding author.

\*\* Corresponding author.

\*\*\* Corresponding author.

\*\*\*\* Corresponding author.

E-mail addresses: [huangyan@scu.edu.cn](mailto:huangyan@scu.edu.cn) (Y. Huang), [luzhiyun@scu.edu.cn](mailto:luzhiyun@scu.edu.cn) (Z. Lu), [h-sasabe@yz.yamagata-u.ac.jp](mailto:h-sasabe@yz.yamagata-u.ac.jp) (H. Sasabe), [kid@yz.yamagata-u.ac.jp](mailto:kid@yz.yamagata-u.ac.jp) (J. Kido).

<sup>1</sup> The first two authors contributed equally to this work.

construct high performance photovoltaic materials.

So far, our group focused on the molecular tailoring of D' segments in USQs, especially for the end-capping units [14–17]. However, another side (D subunit) is also extremely important for USQs materials. 2,3,3-Trimethylindolenine and 2-methylbenzothiazole as a promising donor subunits widely used in symmetrical squaraines with excellent hole mobilities [10,21–23]. Hence, 2,3,3-trimethylindolenine and 2-methylbenzothiazole were used as D subunits, 5-(1,3,3a,8b-tetrahydrocyclopenta[*b*]indolyl)benzene-1,3-diol group acted as D' segment [17], two novel USQs materials, namely USQ-11 and USQ-12 (shown in Fig. 1), were designed and synthesized to investigate the effect of different D subunits on the electronic and steric effect of USQs for the first time. Their optical, electrochemical, quantum chemical, hole mobility, morphology and photovoltaic properties were investigated further below.

## 2. Experimental section

### 2.1. Instruments and characterization

$^1\text{H}$  NMR and  $^{13}\text{C}$  NMR spectra were measured using a Bruker Avance AV II-400 MHz spectrometer, and the chemical shifts were recorded in units of ppm with TMS as the internal standard. High resolution mass spectra was obtained from a Shimadzu LCMS-IT-TOF. Thermogravimetry analysis (TGA) was performed on a Perkin-Elmer TGA Q500 instrument in an atmosphere of  $\text{N}_2$  at a heating rate of  $10\text{ }^\circ\text{C min}^{-1}$ . The purity of USQs compounds were measured by EZChrom Elite for Hitachi high performance liquid chromatography (DAD and RI detector). Electronic absorption spectra of both solution and thin-films of the USQs were recorded using a Perkin Elmer Lambda 950 UV-Vis scanning spectrophotometer. The ground-state geometries and electronic structures of the USQs were calculated with Gaussian 09 software, using density functional theory (DFT) based on B3LYP/6-31G(d) and B3LYP/6-311G(d, p) levels. The solution samples were prepared in chloroform solution at a concentration of  $3.00 \times 10^{-6}\text{ mol L}^{-1}$ , while the thin film samples were obtained by spin-coating from chloroform solution ( $4\text{ mg mL}^{-1}$ , 1500 rpm/45 s) on quartz substrates. Cyclic voltammetry measurements were carried out in  $2.5 \times 10^{-4}\text{ mol L}^{-1}$  anhydrous dichloromethane (DCM) with tetrabutyl ammonium perchlorate ( $\text{Bu}_4\text{NClO}_4$ ) under an argon atmosphere at a scan rate of  $50\text{ mV s}^{-1}$  using a LK 2005A electrochemical workstation. The CV system was constructed using a Pt disk, a Pt wire, and a Ag/AgNO<sub>3</sub> ( $0.1\text{ mol L}^{-1}$  in acetonitrile) electrode as the working electrode, counter electrode and reference electrode, respectively, and the potential of the Ag/AgNO<sub>3</sub> reference electrode was internally calibrated using the ferrocene/ferrocenium redox couple ( $\text{Fc}/\text{Fc}^+$ ), which has a known reduction potential of  $-4.80\text{ eV}$  relative to vacuum level. The morphologies of the active layers were analyzed by atomic force microscopy (AFM) in tapping mode in air under room temperature using Bruker instrument, the active layers were fabricated on ITO/MoO<sub>3</sub> (8 nm) substrates.

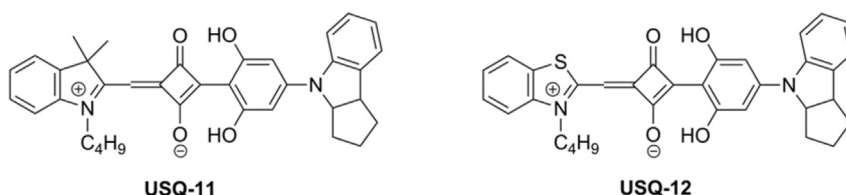


Fig. 1. Chemical structure of the USQs compounds.

### 2.2. Fabrication of organic solar cells and characterization

Bulk-heterojunction small molecule organic solar cells were fabricated with indium-tin-oxide (ITO) coated glass as substrate. The sheet resistance of ITO is  $15\ \Omega\ \text{sq}^{-1}$ . Patterned ITO-coated glass substrates were sequentially cleaned using detergent, deionized water, acetone, and isopropanol in an ultrasonic bath for 30 min each. The cleaned substrates were dried in an oven at  $65\text{ }^\circ\text{C}$  for 12 h before using. The substrates were treated by UV-ozone for 20 min, then immediately transferred into a high vacuum chamber for deposition of 8 nm MoO<sub>3</sub> at pressures of less than  $1 \times 10^{-4}\text{ Pa}$  with a rate of  $0.2\ \text{\AA s}^{-1}$ . Subsequently, photoactive layers (thickness: 50 nm) were fabricated by spin-coating a blend of the USQs and PC<sub>71</sub>BM in chloroform with total concentration of  $20\text{ mg mL}^{-1}$  under a  $\text{N}_2$ -filling glovebox at  $35\text{ }^\circ\text{C}$ , then the blend films were thermal annealed at  $80\text{ }^\circ\text{C}$  for 10 min. Finally, the substrates were transferred back to the high-vacuum chamber, where BCP (6 nm) and Al (100 nm) were deposited as the top electrode at pressures of less than  $8 \times 10^{-5}\text{ Pa}$  with a rate of  $0.20\ \text{\AA s}^{-1}$  and  $2 \times 10^{-4}\text{ Pa}$  with a rate of  $1.5\text{--}4.0\ \text{\AA s}^{-1}$ , respectively, resulting in a final SMOSCs with the structure of ITO/MoO<sub>3</sub>(8 nm)/USQs:PC<sub>71</sub>BM(50 nm)/BCP(6 nm)/Al(100 nm). The active area of OSC cell is  $9\text{ mm}^2$ . Current density-voltage (*J*-*V*) and external quantum efficiency (EQE) characterizations of organic solar cells were performed on a CEP-2000 integrated system manufactured by Bunkoukeiki Co. The integration of EQE data over an AM 1.5G solar spectrum yielded calculated  $J_{\text{sc}}$  values with an experimental variation of less than 6% relative to the  $J_{\text{sc}}$  measured under  $100\text{ mW cm}^{-2}$  simulated AM 1.5G light illumination. Hole-only devices were fabricated with the structure of ITO/MoO<sub>3</sub>(8 nm)/USQ-11(47 nm) or USQ-12(60 nm) or USQs:PC<sub>71</sub>BM(50 nm)/MoO<sub>3</sub>(8 nm)/Al(100 nm).

### 2.3. Synthesis

Compound 3a and 3,4-diethoxy-cyclobut-3-ene-1,2-dione were prepared according to the procedures described in the literature [14,17]. The synthetic details of intermediates 1a, 2a, 1b, 2b, 1c and 2c were shown in Support Information. *n*-Butanol and toluene were distilled from sodium freshly prior to use. All other chemicals were obtained from commercial sources and used as-received without further purification.

#### 2.3.1. 4-((1-Butyl-3,3-dimethyl-3H-indol-1-ium-2-yl)methylene)-2-(2,6-dihydroxy-4-(1,3,3a,8b-tetrahydrocyclopenta[*b*]indol-4(2H-yl)phenyl)-3-oxocyclobut-1-enolate (USQ-11)

A mixture of compound 3a (596 mg, 2.22 mmol) and 1c (622 mg, 2.00 mmol) in *n*-butanol (50 mL) and toluene (50 mL) were added into a round bottom flask. The mixture was refluxed with a Dean-Stark apparatus for 36 h. After reaction was cooled down, the solvents were removed under reduced pressure. This crude product was purified by silica gel chromatography using dichloromethane/methanol (50:1, v/v) as the eluent to afford green solid. The solid was recrystallized from a 1:6 vol ratio of dichloromethane and methanol mixture to afford green crystals USQ-11 (817 mg, 73%),

mp. 214–215 °C.  $^1\text{H}$  NMR (400 MHz,  $\text{CDCl}_3$ , ppm)  $\delta$ : 12.33 (2H, s, –OH), 7.43 (1H, d,  $J = 7.2$  Hz, ArH), 7.38 (2H, d,  $J = 8.4$  Hz, ArH), 7.29 (1H, t,  $J = 7.2$  Hz, ArH), 7.18–7.10 (3H, m, ArH), 6.95 (1H, t,  $J = 7.2$  Hz, ArH), 6.34 (2H, s, ArH), 5.92 (1H, s, =CH–), 4.70 (1H, t,  $J = 7.2$  Hz, –NCH–), 4.10 (2H, t,  $J = 7.6$  Hz, –NCH<sub>2</sub>–), 3.91 (1H, t,  $J = 7.2$  Hz, =CH–), 2.10–2.01 (2H, m, –CH<sub>2</sub>–), 2.00–1.91 (2H, m, –CH<sub>2</sub>–), 1.86–1.78 (2H, m, –CH<sub>2</sub>–), 1.77 (6H, s, –CH<sub>3</sub>), 1.70–1.62 (1H, m, –CH<sub>2</sub>–), 1.53–1.43 (2H, m, –CH<sub>2</sub>–), 1.42–1.35 (1H, m, –CH<sub>2</sub>–), 1.03 (3H, t,  $J = 7.6$  Hz, –CH<sub>3</sub>);  $^{13}\text{C}$  NMR (100 MHz,  $\text{CDCl}_3$ , ppm)  $\delta$ : 173.7, 170.3, 162.9, 152.6, 144.0, 142.6, 141.6, 136.9, 128.2, 127.4, 125.5, 124.8, 122.5, 122.3, 113.6, 110.7, 104.7, 96.7, 87.7, 68.6, 50.3, 45.5, 44.2, 34.6, 33.8, 29.4, 26.6, 24.3, 20.3, 13.8; HR-MS (ESI):  $m/z$  [M+H] 561.2753, calcd.: 561.2756; purity: 99.2% (HPLC, eluent: THF/CH<sub>3</sub>CN = 1/9); elemental anal. calcd for C<sub>36</sub>H<sub>36</sub>N<sub>2</sub>O<sub>4</sub>: C 77.12, H 6.47, N 5.00; found, C 76.71, H 6.70, N 4.91.

### 2.3.2. 4-((3-Butylbenzo[d]thiazol-3-ium-2-yl)methylene)-2-(2,6-dihydroxy-4-(1,3,3a,8b-tetra-hydrocyclopenta[b]indol-4(2H)-yl)phenyl)-3-oxocyclobut-1-enolate (USQ-12)

USQ-12 was obtained from the reaction of compound 3a (297 mg, 1.11 mmol) and 2c (300 mg, 1.00 mmol) according to the procedure described for the synthesis of USQ-11. The solid was recrystallized from a 1:4 vol ratio of dichloromethane and methanol mixture to afford green solid (270 mg, 49%), mp. 240–241 °C.  $^1\text{H}$  NMR (400 MHz,  $\text{CDCl}_3$ , ppm)  $\delta$ : 7.73 (1H, d,  $J = 7.6$  Hz, ArH), 7.47 (1H, t,  $J = 8.0$  Hz, ArH), 7.38–7.31 (3H, m, ArH), 7.16 (2H, t,  $J = 7.2$  Hz, ArH), 6.92 (1H, t,  $J = 7.6$  Hz, ArH), 6.26 (2H, d,  $J = 3.2$  Hz, ArH), 6.06 (1H, s, =CH–), 4.66 (1H, t,  $J = 8.0$  Hz, –NCH–), 4.29 (2H, t,  $J = 7.6$  Hz, –NCH<sub>2</sub>–), 3.90 (1H, t,  $J = 8.0$  Hz, =CH–), 2.09–1.99 (2H, m, –CH<sub>2</sub>–), 1.98–1.91 (2H, m, –CH<sub>2</sub>–), 1.89–1.81 (2H, m, –CH<sub>2</sub>–), 1.70–1.62 (1H, m, –CH<sub>2</sub>–), 1.53–1.43 (2H, m, –CH<sub>2</sub>–), 1.42–1.36 (1H, m, –CH<sub>2</sub>–), 1.05 (3H, t,  $J = 7.6$  Hz, –CH<sub>3</sub>);  $^{13}\text{C}$  NMR (100 MHz,  $\text{CDCl}_3$ , ppm)  $\delta$ : 182.1, 180.9, 169.8, 164.6, 164.3, 161.6, 161.3, 150.7, 144.5, 140.3, 136.5, 128.9, 128.1, 127.3, 126.1, 124.8, 122.7, 121.6, 113.1, 112.7, 103.3, 96.7, 96.5, 88.2, 68.4, 47.3, 45.4, 34.7, 34.0, 29.9, 24.3, 20.2, 13.7; HR-MS (ESI):  $m/z$  [M+H] 551.2005, calcd.: 551.2005; purity: 99.6% (HPLC, eluent: THF/CH<sub>3</sub>CN = 1/9); elemental anal. calcd for C<sub>33</sub>H<sub>30</sub>N<sub>2</sub>O<sub>4</sub>S: C 71.98, H 5.49, N 5.09, S 5.82; found, C 71.46, H 5.58, N 4.91, S 5.56.

## 3. Results and discussion

### 3.1. Synthesis and characterization

The synthetic routes to the USQs compounds are illustrated in Scheme 1. Intermediate 1b and 2b were synthesized similarly starting with Knoevenagel condensation reaction of compounds 1a and 2a, respectively, with the 3,4-diethoxy-cyclobut-3-ene-1,2-dione. Then intermediate 1c and 2c were obtained by hydrolysis of compounds 1b and 2b, respectively. Next, they were further condensed with compound 3a to afford the unsymmetrical squaraines USQ-11 and USQ-12. Both of the two objective USQs compounds displayed good solubility in common organic solvents, such as chloroform (>10 mg mL<sup>−1</sup>) and 1,2-dichlorobenzene (>15 mg mL<sup>−1</sup>). Moreover, high quality thin films of the USQs compounds could be obtained through spin-coating from solution, suggesting that they are very suitable for solution-processing. As shown in Fig. S1 (shown in SI), both of the two USQs compounds exhibited excellent thermal stability over 270 °C under N<sub>2</sub> atmosphere (vide Table 1).

### 3.2. Optical properties

The UV-vis absorption spectra of the USQs compounds in chloroform solution and thin films are shown in Fig. 2, and the data

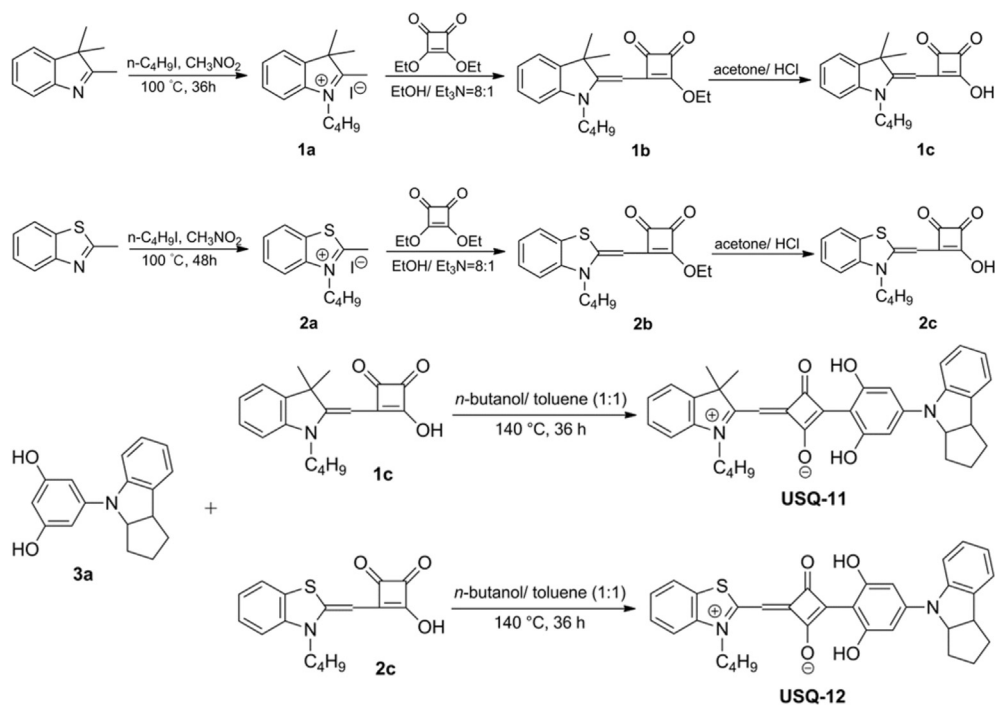
are summarized in Table 1. In dilute solution, USQ-11 and USQ-12 exhibited very similar absorption profiles with the wavelength of maxima absorption ( $\lambda_{\text{max}}$ ) of ~667 nm and full width half maxima (FWHM) of ~1000 cm<sup>−1</sup>, with a considerably high molar extinction coefficient of > 10<sup>5</sup> M<sup>−1</sup> cm<sup>−1</sup>. In comparison with the absorption in solution, the absorption bands of the thin films of the two USQs compounds were significantly broadened (FWHM: from 900 to 3910 cm<sup>−1</sup> for USQ-11, from 1080 to 5060 cm<sup>−1</sup> for USQ-12). However, quite different shapes of absorption bands could be observed in thin film, the absorption maximum of the USQ-11 thin film was red-shifted by 31 nm from the monomer peak in solution; while 47 nm blue-shift could be observed in the USQ-12 thin film. These drastic spectral changes are attributed to squaraines aggregations. As we know, squaraines showed pronounced aggregation features as they are known to form H- and J-aggregation in solid films [24,25]. The H-aggregation displayed a blue-shift in the absorption maximum, which contributed to only a moderate increase in the  $J_{\text{sc}}$ ; while the J-aggregation exhibited a red-shift in the absorption maximum that resulted in a significantly increase in the  $J_{\text{sc}}$  [11,26–28]. Thus, for USQ-11, the absorption peak exhibited a bathochromic shift from 667 nm to 698 nm, which is probably due to J-aggregation; while for USQ-12, the absorption peak showed a hypsochromic shift from 668 nm to 621 nm, which is attributed to H-aggregation. The branched two methyl groups of indolenine hindered the  $\pi$ - $\pi$  stacking of USQ-11, thereby enhancing J-aggregation; on the contrary, the benzothiazole segment showed a planar structure, which is very beneficial for formation H-aggregation [29]. Therefore, the totally different solid state aggregations were attributed to their distinct steric effects. Determined by the onset position of the absorption spectra of the USQs in the thin films, optical band-gaps were calculated to be 1.53 and 1.52 eV, respectively, for USQ-11 and USQ-12.

### 3.3. Electrochemistry properties

To estimate the energy level of the HOMO of these USQs compounds, their electrochemical properties were investigated by cyclic voltammetry. As shown in Fig. 3 and Table 2, during anodic scan, quasireversible oxidation processes could be observed in the two USQs compounds, and their Eonset ox values were determined to be 0.30 and 0.23 V relative to Fc/Fc<sup>+</sup> for USQ-11 and USQ-12, respectively. Accordingly, the HOMO energy levels of USQ-11 and USQ-12 were calculated to be −5.10 and −5.03 eV, respectively, by comparison with the Fc/Fc<sup>+</sup> redox couple whose energy level is −4.80 eV in vacuum [30]. In comparison with the USQ-11, the USQ-12 possessed 0.07 eV higher HOMO energy level, which may be attributed to its stronger electron-donating capability of 2-methylbenzothiazole than that of 2,3,3-trimethylindolenine group. Therefore, higher  $V_{\text{oc}}$  could be expected when USQ-11 was used as electron-donors materials to fabricate OSCs [31]. Moreover, the LUMO energy levels of USQ-11 and USQ-12 were calculated to be −3.57 and −3.51 eV, respectively, which are deduced from their HOMO levels and corresponding optical band-gaps [15].

### 3.4. DFT calculation

To gain further insights into the effect of different D subunits on the electronic properties of these USQs compounds, quantum chemical DFT calculations were performed. As shown in Fig. 4, both of the two USQs shown similar electronic structures, their HOMOs are delocalized on the whole molecular skeleton, while their LUMOs exhibited a few difference, since the indoline groups contributed much to the HOMO but little to the LUMO. As shown in Table 2, the HOMO energy levels of USQ-11 and USQ-12 were calculated to be −5.19 and −5.12 eV, respectively, and the LUMO



Scheme 1. Synthetic routes to the USQs compounds.

Table 1  
Optical properties of the USQs compounds.

Compound	Absorption $\lambda_{\text{abs max}}$ (nm)		FWHM (cm <sup>-1</sup> )		$E_g^{\text{opt}}$ (eV)	Td (°C)
	Solution ( $\epsilon 10^5 \text{ M}^{-1} \text{ cm}^{-1}$ )	Film	Solution	Film		
USQ-11	667 (2.41)	698, 648	900	3910	1.53	271
USQ-12	668 (1.91)	672, 621	1080	5060	1.52	283

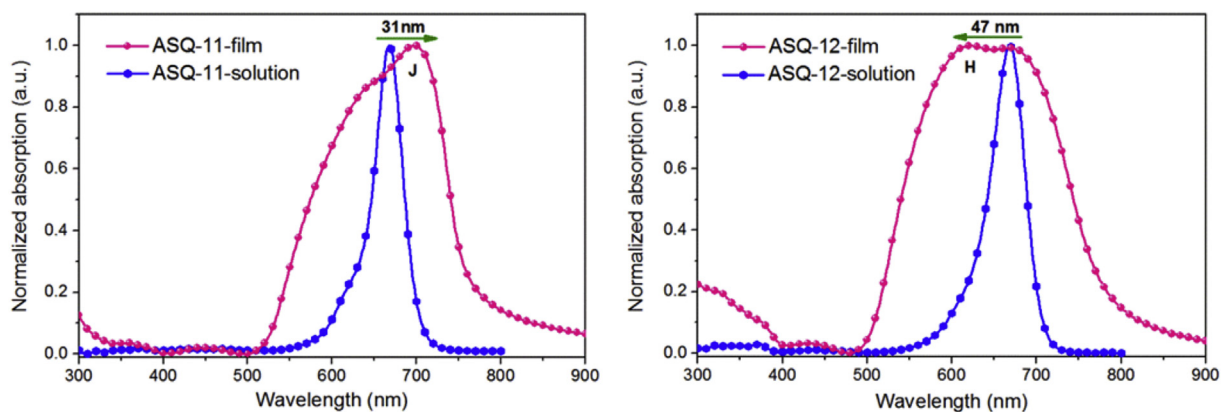


Fig. 2. Absorption spectra of the USQs compounds in solution and thin films.

energy levels of USQ-11 and USQ-12 were calculated to be  $-2.93$  and  $-2.87$  eV, respectively, which well reproduce their corresponding experimental values, indicating that these computational results are reliable.

Moreover, as shown in Fig. 5, although the dipole moment of both compounds pointed in the same direction, their magnitude was quite different. USQ-11 (dipole moment 3.24 D) exhibited in fact a sizably less pronounced charge transfer character than that of USQ-12 (dipole moment 5.23 D). Such difference might explain

why USQ-12 mostly shown H- aggregation behavior [29], a geometry preferred in the presence of strong dipole-dipole coupling, which can endow the compound with a more enhanced higher hole mobility [22,32,33].

### 3.5. Hole mobility and morphology

The hole mobility of the two pristine USQs as well as the USQs/PC<sub>71</sub>BM (1:5, wt%) blend film samples were evaluated by the space

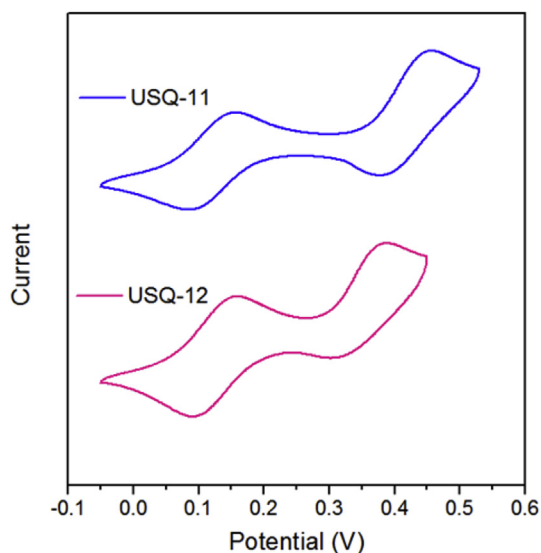


Fig. 3. Cyclic voltammogram of the USQs compounds.

**Table 2**  
Cyclic voltammetry and DFT calculated data for the USQs compounds.

Compound	$E_{ox}^{onest}$ (V)	HOMO <sup>a</sup> (eV)	LUMO <sup>b</sup> (eV)	HOMO <sup>c</sup> (eV)	LUMO <sup>c</sup> (eV)	$\mu_g^c$ (D)
USQ-11	0.30	-5.10	-3.57	-5.19	-2.93	3.24
USQ-12	0.23	-5.03	-3.51	-5.12	-2.87	5.23

<sup>a</sup> HOMO values derived from cyclic voltammetry measurements.

<sup>b</sup> LUMO =  $E_g^{opt}$  + HOMO.

<sup>c</sup> Data derived from DFT calculation.

charge limited current method [34], and the  $J$ - $V$  characteristics of the devices are shown in Fig. 6. The hole mobility of the USQ-11 neat film was calculated to be  $4.33 \times 10^{-5} \text{ cm}^2 \text{ V}^{-1} \text{ s}^{-1}$ , which was much lower than that of the USQ-12 ( $8.61 \times 10^{-5} \text{ cm}^2 \text{ V}^{-1} \text{ s}^{-1}$ ), which was ascribed to its much higher dipole moment. However, the hole mobility of the USQ-11/PC<sub>71</sub>BM blend film was calculated to be  $2.03 \times 10^{-5} \text{ cm}^2 \text{ V}^{-1} \text{ s}^{-1}$ , which is nearly 4 times higher than that of the USQ-12/PC<sub>71</sub>BM ( $5.10 \times 10^{-6} \text{ cm}^2 \text{ V}^{-1} \text{ s}^{-1}$ ). The higher mobility in blend films is beneficial for  $J_{sc}$ .

The morphologies of the blend films were investigated by AFM. As shown in Fig. 7, both of the two USQs/PC<sub>71</sub>BM blend films exhibited similar root mean square (RMS) of 1.32–1.45 nm, however, the USQ-12/PC<sub>71</sub>BM blend films displayed quite larger phase separation than that of the USQ-11/PC<sub>71</sub>BM, which could be the result of limited mixing with PC<sub>71</sub>BM. Therefore, the low hole mobility of the USQ-12/PC<sub>71</sub>BM should be ascribed to the poor miscibility.

### 3.6. Organic solar cells

To evaluate the photovoltaic performance of the two USQs compounds, devices with structure of ITO/MoO<sub>3</sub> (8 nm)/USQs/PC<sub>71</sub>BM (50 nm)/BCP (6 nm)/Al (100 nm) have been fabricated. The photovoltaic properties of the OSCs devices are listed in Table 3, the corresponding current density-voltage ( $J$ - $V$ ) curves, and external quantum efficiency (EQE) plots are displayed in Figs. 8 and 9, respectively. Firstly, the effect of different blend ratios of USQs/PC<sub>71</sub>BM on photovoltaic properties were investigated. For the USQ-11 compound, when the USQ-11/PC<sub>71</sub>BM blend ratios increased from 1:1 to 1:3, the  $J_{sc}$  and FF of the devices improved significantly from 6.41 to 10.21 mA cm<sup>-2</sup> and 0.40 to 0.47, respectively, while no distinct changes can be observed for the  $V_{oc}$  of the devices; when

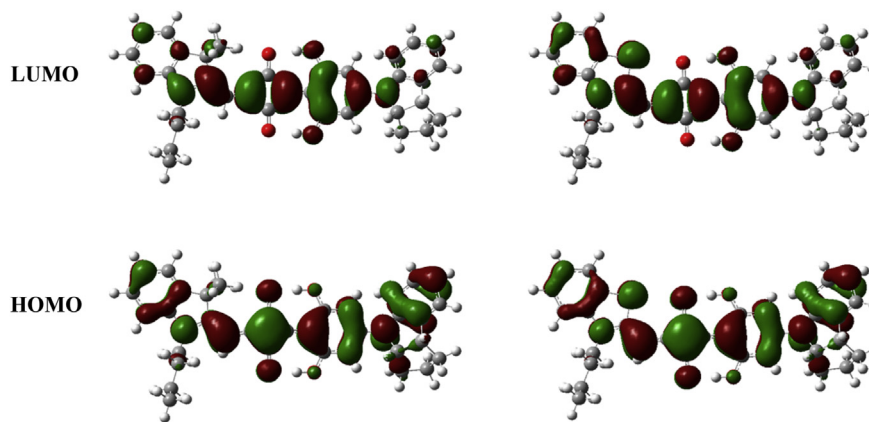


Fig. 4. The electron density distributions of USQ-11 (left) and USQ-12 (right).

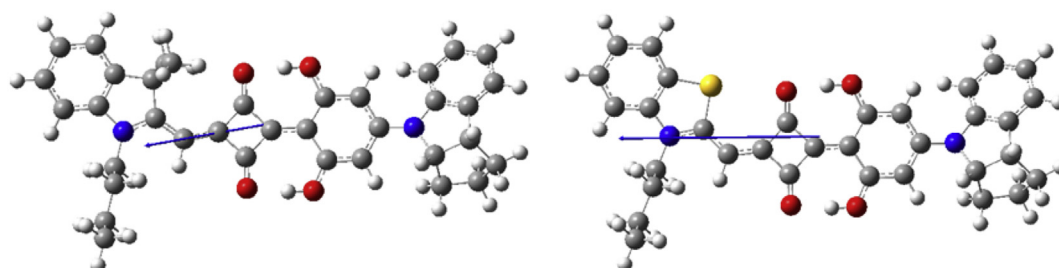


Fig. 5. The dipole moments of USQ-11 (left) and USQ-12 (right).

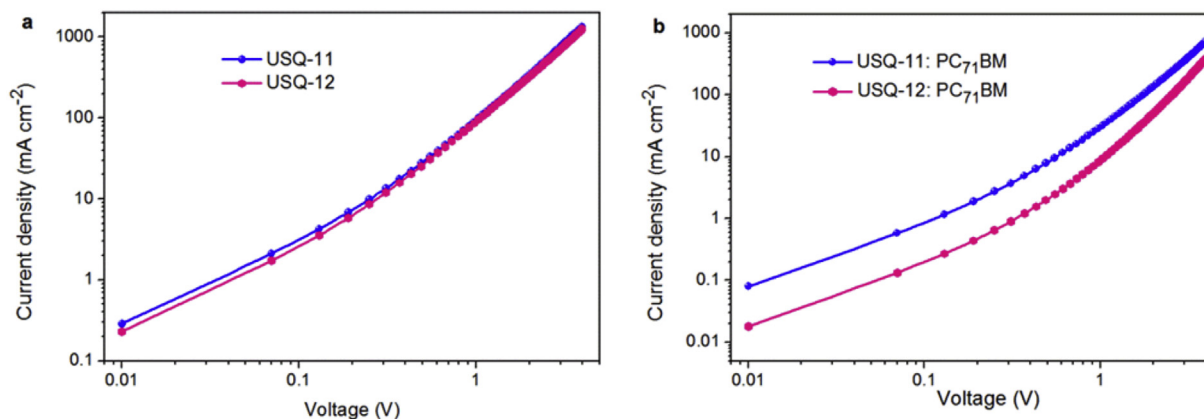


Fig. 6. *J*-*V* characteristic of the hole-only devices using the neat film of USQs (a), and USQs/PC<sub>71</sub>BM (1:5, wt%) blend films (b) as active layer.

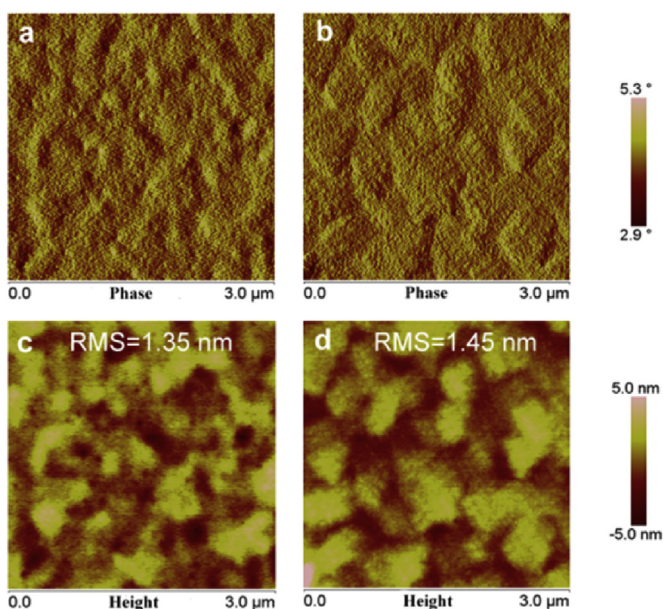


Fig. 7. AFM phase images and height images of the USQs/PC<sub>71</sub>BM (1:5, wt%) blend films, USQ-11/PC<sub>71</sub>BM (a,c) and USQ-12/PC<sub>71</sub>BM (b,d).

the blend ratios increased further from 1:3 to 1:7, there are not distinct changes for the  $V_{oc}$ ,  $J_{sc}$  and FF of the devices. Thus, the best blend ratio of USQ-11/PC<sub>71</sub>BM-based device was 1:5, with  $V_{oc}$  of 0.86 V,  $J_{sc}$  of 10.34 mA cm<sup>-2</sup>, FF of 0.48 and PCE of 4.27%. While for the USQ-12/PC<sub>71</sub>BM system, the blend ratios increased from 1:1 to

1:3, the  $J_{sc}$  and FF of the devices enhanced from 7.15 to 9.34 mA cm<sup>-2</sup> and 0.41 to 0.45, respectively, and with a further increased blend ratios from 1:3 to 1:7, the  $J_{sc}$  and FF of the devices gradually decreased from 9.34 to 8.44 mA cm<sup>-2</sup> and 0.45 to 0.41, respectively, the PCE dropped to 2.53%. Thus, the highest PCE (3.03%) was obtained when the USQ-12/PC<sub>71</sub>BM blend ratio was 1:3, with  $V_{oc}$  of 0.72 V,  $J_{sc}$  of 9.34 mA cm<sup>-2</sup> and FF of 0.45.

To investigate the effect of different D subunits on the photovoltaic properties of the two USQs compounds, the data of devices fabricated in USQs/PC<sub>71</sub>BM blend ratio of 1:5 was used for discussion. The  $V_{oc}$  of USQ-11-based device was 0.86 V, 0.14 V higher than that of the USQ-12. The results are not very consistent with the HOMO energy levels of the USQ-11 as just 0.07 eV lower than that of the USQ-12. This indicated that there are large voltage losses in the USQ-12-based devices. Theoretically, the  $V_{oc}$  of OSCs is limited by the difference between the HOMO of the donor and the LUMO of the acceptor [31]. However, charge transfer states, disorder induced changes in the hole and electron quasi-Fermi levels, and electronic coupling between the donor's ground state have been shown to cause losses in the  $V_{oc}$  [35–38]. In addition to the much enhanced  $V_{oc}$ , the USQ-11-based device also exhibited quite higher  $J_{sc}$  (10.34 mA cm<sup>-2</sup>) than that of the USQ-12 (8.97 mA cm<sup>-2</sup>). In principle,  $J_{sc}$  correlates highly with the light-harvesting capability, carrier mobility, and the morphology of the active layer [39–41]. To elucidate the origin of the enhanced  $J_{sc}$  in USQ-11-based device, the EQE plots of the two devices were recorded. As shown in Fig. 9, the USQ-11-based device exhibited a broader spectral response and higher EQE values than that of USQ-12. Moreover, the hole mobility of USQ-11/PC<sub>71</sub>BM blend film displayed nearly 4 times higher than that of the USQ-12/PC<sub>71</sub>BM blend film. Thus, compared with the USQ-12-based device, the enhanced  $J_{sc}$  of USQ-11-device should be ascribed to the higher hole mobility of the blend film, better phase separation as well as the broader absorption band. Therefore, 2,3,3-trimethylindolenine subunit substituted USQ-11 displayed much higher photovoltaic performance (PCE = 4.27%) than that of 2-methylbenzothiazole subunit substituted USQ-12 (PCE = 2.78%).

#### 4. Conclusion

In conclusion, the effect of D subunits on the optoelectronic properties of small molecules have been evaluated by comparing the two USQs compounds. By changing the different D subunits attached to the squaric acid core from 2,3,3-trimethylindolenine to 2-methylbenzothiazole, two novel USQs compounds, namely USQ-11 and USQ-12, were designed and synthesized. Both of them displayed similar absorption bands in their solutions, however,

Table 3  
Photovoltaic performances of SMOSCs based on USQs: PC<sub>71</sub>BM.

Donor	Ratio (D:A)	$V_{oc}^a$ (V)	$J_{sc}^a$ (mA cm <sup>-2</sup> )	FF <sup>a</sup>	PCE <sup>a</sup> (%)
USQ-11	1:1	0.86 (0.86)	6.41 (6.36)	0.40 (0.40)	2.20 (2.19)
	1:3	0.85 (0.85)	10.21 (10.00)	0.47 (0.47)	4.08 (4.00)
	1:5	0.86 (0.86)	10.34 (10.26)	0.48 (0.48)	4.27 (4.24)
	1:7	0.86 (0.86)	10.33 (10.06)	0.47 (0.47)	4.17 (4.07)
USQ-12	1:1	0.73 (0.73)	7.15 (6.85)	0.41 (0.41)	2.14 (2.05)
	1:3	0.72 (0.72)	9.34 (9.12)	0.45 (0.45)	3.03 (2.95)
	1:5	0.72 (0.72)	8.97 (8.91)	0.43 (0.43)	2.78 (2.76)
	1:7	0.73 (0.73)	8.44 (8.43)	0.41 (0.40)	2.53 (2.46)

<sup>a</sup> The first values are the best data obtained, while the values in parentheses are average values from 4 devices.

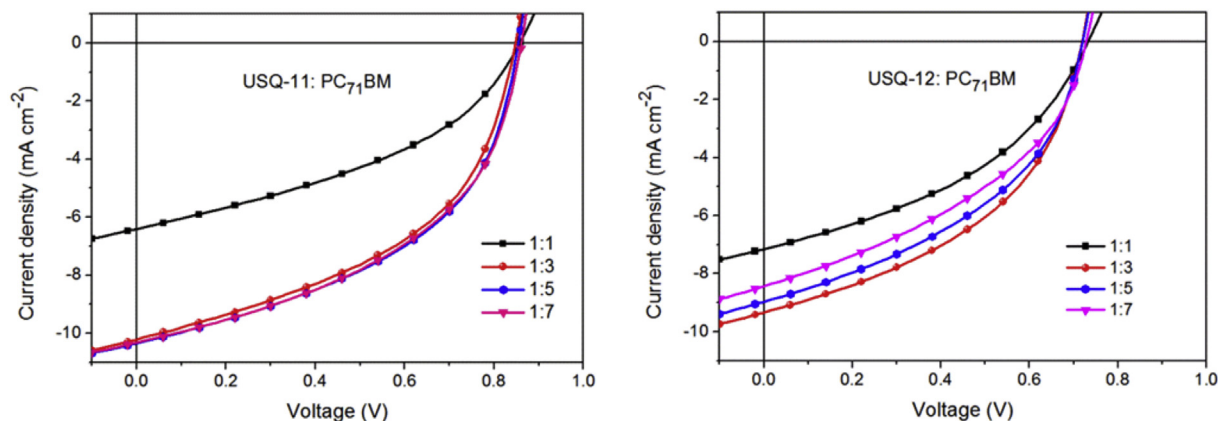


Fig. 8. *J*-*V* curves characteristics of SMOSCs devices with different blend ratios.

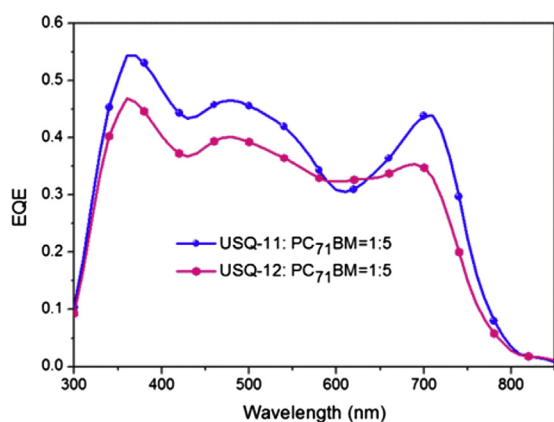


Fig. 9. EQE curves of SMOSCs devices.

significantly different absorption bands could be observed in their thin films as their totally different H- and J-aggregations, which should be attributed to their distinct dipole moments and steric effects. In comparison with the USQ-11 compound, the USQ-12 exhibited 0.07 eV higher HOMO energy levels, and much higher dipole moment and steric effects. Although the hole mobility of the USQ-11 neat film was lower than that of the USQ-12, the hole mobility of the USQ-11/PC<sub>71</sub>BM blend film was quite higher than that of the USQ-12/PC<sub>71</sub>BM, which was ascribed to its smaller domains size. Therefore, solution-processed BHJ-SMOSCs fabricated with the USQ-11/PC<sub>71</sub>BM (1:5, wt%) exhibited much higher PCE (4.27%) than that of the USQ-12/PC<sub>71</sub>BM (2.78%), which was attributed to its simultaneously enhanced  $V_{oc}$ ,  $J_{sc}$  and FF. These preliminary results demonstrate that D subunit plays a quite important role in the USQs, and 2,3,3-trimethylindolenine unit should be a much better D subunit for construction of high performance squaraines photovoltaic materials.

### Acknowledgement

We acknowledge the financial support for this work by the China Scholarship Council and National Natural Science Foundation of China (No. 51573108, 21190031, 21372168, 21432005). We are grateful to the Comprehensive Training Platform of Specialized Laboratory, College of Chemistry, Sichuan University for providing NMR and HR-MS data for the intermediates and objective USQs compounds.

### Appendix A. Supplementary data

Supplementary data related to this article can be found at <http://dx.doi.org/10.1016/j.orgel.2016.02.009>.

### References

- [1] J. Roncali, P. Leriche, P. Blanchard, Molecular materials for organic photovoltaics: small is beautiful, *Adv. Mater.* 26 (2014) 3821–3838.
- [2] L. Dou, Y. Liu, Z. Hong, G. Li, Y. Yang, Low-bandgap near-IR conjugated polymers/molecules for organic electronics, *Chem. Rev.* 115 (2015) 12633–12665.
- [3] B. Kan, M. Li, Q. Zhang, F. Liu, X. Wan, Y. Wang, W. Ni, G. Long, X. Yang, H. Feng, Y. Zuo, M. Zhang, F. Huang, Y. Cao, T.P. Russell, Y. Chen, A series of simple oligomer-like small molecules based on oligothiophenes for solution-processed solar cells with high efficiency, *J. Am. Chem. Soc.* 137 (2015) 3886–3893.
- [4] J. Huang, T. Goh, X. Li, M.Y. Sfeir, E.A. Bielinski, S. Tomasulo, M.L. Lee, N. Hazari, A.D. Taylor, Polymer bulk heterojunction solar cells employing Förster resonance energy transfer, *Nat. Phot.* 7 (2013) 479–485.
- [5] Y. Fu, D.A. da Silva Filho, G. Sini, A.M. Asiri, S.G. Aziz, C. Risko, J. Brédas, Structure and disorder in squaraine-C60 organic solar cells: a theoretical description of molecular packing and electronic coupling at the donor-acceptor interface, *Adv. Funct. Mater.* 24 (2014) 3790–3798.
- [6] H. Sasabe, T. Igarashi, Y. Sasaki, G. Chen, Z. Hong, J. Kido, Soluble squaraine derivatives for 4.9% efficient organic photovoltaic cells, *RSC Adv.* 4 (2014) 42804–42807.
- [7] S. Bellani, A. Iacchetti, M. Porro, L. Beverina, M.R. Antognazza, D. Natali, Charge transport characterization in a squaraine-based photodetector by means of admittance spectroscopy, *Org. Electron.* 22 (2015) 56–61.
- [8] G. Chen, H. Sasabe, T. Igarashi, Z. Hong, J. Kido, Squaraine dyes for organic photovoltaic cells, *J. Mater. Chem. A* 3 (2015) 14517–14534.
- [9] S. Paek, H. Choi, H. Jo, K. Lee, K. Song, S.A. Siddiqui, G.D. Sharma, J. Ko, A new unsymmetrical near-IR small molecule with squaraine chromophore for solution processed bulk heterojunction solar cells, *J. Mater. Chem. C* 3 (2015) 7029–7037.
- [10] U. Mayerhoffer, K. Deing, K. Grub, H. Braunschweig, K. Meerholz, F. Würthner, Outstanding short-circuit currents in BHJ solar cells based on NIR-absorbing acceptor-substituted squaraines, *Angew. Chem. Int. Ed.* 48 (2009) 8776–8779.
- [11] K.C. Deing, U. Mayerhoffer, F. Würthner, K. Meerholz, Aggregation-dependent photovoltaic properties of squaraine/PC<sub>61</sub>BM bulk heterojunctions, *Phys. Chem. Chem. Phys.* 14 (2012) 8328–8334.
- [12] L. Beverina, R. Ruffo, M.M. Salamone, E. Ronchi, M. Binda, D. Natali, M. Sampietro, Panchromatic squaraine compounds for broad band light harvesting electronic devices, *J. Mater. Chem.* 22 (2012) 6704–6710.
- [13] S. Seulgi, C. Hyunbong, K.M. Haye, K. Chulwoo, P. Sanghyun, N. Cho, S. Kihyung, L.K. Jae, K. Jaeyung, Novel unsymmetrical push-pull squaraine chromophores for solution processed small molecule bulk heterojunction solar cells, *Sol. Energy Mater. Sol. Cells* 98 (2012) 224–232.
- [14] D. Yang, Q. Yang, L. Yang, Q. Luo, Y. Huang, Z. Lu, S. Zhao, Novel high performance asymmetrical squaraines for small molecule organic solar cells with a high open circuit voltage of 1.12 V, *Chem. Commun.* 49 (2013) 10465–10467.
- [15] D. Yang, Q. Yang, L. Yang, Q. Luo, Y. Chen, Y. Zhu, Y. Huang, Z. Lu, S. Zhao, A low bandgap asymmetrical squaraine for high-performance solution-processed small molecule organic solar cells, *Chem. Commun.* 50 (2014) 9346–9348.
- [16] D. Yang, Y. Zhu, Y. Jiao, L. Yang, Q. Yang, Q. Luo, X. Pu, Y. Huang, S. Zhao, Z. Lu, N,N-Diarylamino end-capping as a new strategy for simultaneously enhancing open-circuit voltage, short-circuit current density and fill factor in

- small molecule organic solar cells, *RSC Adv.* 5 (2015) 20724–20733.
- [17] L. Yang, Q. Yang, D. Yang, Q. Luo, Y. Zhu, Y. Huang, S. Zhao, Z. Lu, Marked effects of indolyl vs. indolyl substituent on solid-state structure, carrier mobility and photovoltaic efficiency of asymmetrical squaraine dyes, *J. Mater. Chem. A* 2 (2014) 18313–18321.
- [18] D. Yang, L. Yang, Y. Huang, Y. Jiao, T. Igarashi, Y. Chen, Z. Lu, X. Pu, H. Sasabe, J. Kido, Asymmetrical squaraines bearing fluorine-substituted indoline moieties for high-performance solution-processed small-molecule organic solar cells, *ACS Appl. Mater. Interfaces* 7 (2015) 13675–13684.
- [19] D. Yang, Y. Jiao, L. Yang, Y. Chen, S. Mizoi, Y. Huang, X. Pu, Z. Lu, H. Sasabe, J. Kido, Cyano-substitution on the end-capping group: facile access toward asymmetrical squaraine showing strong dipole–dipole interactions as a high performance small molecular organic solar cells material, *J. Mater. Chem. A* 3 (2015) 17704–17712.
- [20] G. Wei, S. Wang, K. Sun, M.E. Thompson, S.R. Forrest, Solvent-annealed crystalline squaraine: PC<sub>70</sub>BM (1:6) solar cells, *Adv. Energy Mater.* 1 (2011) 184–187.
- [21] U. Mayerhöffer, M. Gsänger, M. Stolte, B. Fimmel, F. Würthner, High-performance organic thin-film transistors of J-stacked squaraine dyes, *J. Am. Chem. Soc.* 136 (2014) 2351–2362.
- [22] A. Liess, L. Huang, A. Arjona-Esteban, A. Lv, M. Gsänger, V. Stepanenko, M. Stolte, F. Würthner, Organic thin film transistors based on highly dipolar donor-acceptor polymethine dyes, *Adv. Funct. Mater.* 25 (2015) 44–57.
- [23] C. Lambert, F. Koch, S.F. Völker, A. Schmiedel, M. Holzapfel, A. Humeniuk, M.I.S. Röhr, R. Mitric, T. Brixner, Energy transfer between squaraine polymer sections: from Helix to Zigzag and all the way back, *J. Am. Chem. Soc.* 137 (2015) 7851–7861.
- [24] K. Liang, K.-Y. Law, D.G. Whitten, Multiple aggregation of surfactant squaraines in Langmuir-Blodgett films and in DMSO-water mixtures, *J. Phys. Chem.* 98 (1994) 13379–13384.
- [25] O.P. Dimitriev, A.P. Dimitriyeva, A.I. Tolmachev, V.V. Kurdyukov, Solvent-induced organization of squaraine dyes in solution capillary layers and adsorbed films, *J. Phys. Chem. B* 109 (2005) 4561–4567.
- [26] G. Chen, H. Sasabe, W. Lu, X. Wang, J. Kido, Z. Hong, Y. Yang, J-aggregation of a squaraine dye and its application in organic photovoltaic cells, *J. Mater. Chem. C* 1 (2013) 6547–6552.
- [27] S. Spencer, H. Hu, Q. Li, H.-Y. Ahn, M. Qaddoura, S. Yao, A. Ioannidis, K. Belfield, C.J. Collison, Controlling J-aggregate formation for increased short-circuit current and power conversion efficiency with a squaraine donor, *Prog. Photovolt.* 22 (2014) 488–493.
- [28] C. Zheng, A.R. Penmetcha, B. Cona, S.D. Spencer, B. Zhu, P. Heaphy, J.A. Cody, C.J. Collison, Contribution of aggregate states and energetic disorder to a squaraine system targeted for organic photovoltaic devices, *Langmuir* 31 (2015) 7717–7726.
- [29] G. Chen, H. Sasabe, Y. Sasaki, H. Katagiri, X.-F. Wang, T. Sano, Z. Hong, Y. Yang, J. Kido, A series of squaraine dyes: effects of side chain and the number of hydroxyl groups on material properties and photovoltaic performance, *Chem. Mater.* 26 (2014) 1356–1364.
- [30] J. Pommerehne, H. Vestweber, W. Guss, R.F. Mahrt, H. Bassler, Efficient two layer leds on a polymer blend basis, *Adv. Mater.* 7 (1995) 551–554.
- [31] M.C. Scharber, D. Mühlbacher, M. Koppe, P. Denk, C. Waldauf, A.J. Heeger, C.J. Brabec, Design rules for donors in bulk-heterojunction solar cells-towards 10% energy-conversion efficiency, *Adv. Mater.* 18 (2006) 789–794.
- [32] H. Bürckstümmer, E.V. Tulyakova, M. Deppisch, M.R. Lenze, N.M. Kronenberg, M. Gsänger, M. Stolte, K. Meerholz, F. Würthner, Efficient solution-processed bulk heterojunction solar cells by antiparallel supramolecular arrangement of dipolar donor-acceptor dyes, *Angew. Chem. Int. Ed.* 50 (2011) 11628–11632.
- [33] C.J. Takacs, Y. Sun, G.C. Welch, L.A. Perez, X. Liu, W. Wen, G.C. Bazan, A.J. Heeger, Solar cell efficiency, self-assembly, and dipole–dipole interactions of isomorphous narrow-band-gap molecules, *J. Am. Chem. Soc.* 134 (2012) 16597–16606.
- [34] Z. He, C. Zhong, X. Huang, W.-Y. Wong, H. Wu, L. Chen, S. Su, Y. Cao, Simultaneous enhancement of open-circuit voltage, short-circuit current density, and fill factor in polymer solar cells, *Adv. Mater.* 23 (2011) 4636–4643.
- [35] T. Sueyoshi, H. Fukagawa, M. Ono, S. Kera, N. Ueno, Low-density band-gap states in pentacene thin films probed with ultrahigh-sensitivity ultraviolet photoelectron spectroscopy, *Appl. Phys. Lett.* 95 (2009) 183303.
- [36] S. Ko, E.T. Hoke, L. Pandey, S. Hong, R. Mondal, C. Risko, Y. Yi, R. Noriega, M.D. McGehee, J.-L. Brédas, A. Salleo, Z. Bao, Controlled conjugated backbone twisting for an increased open-circuit voltage while having a high short-circuit current in poly(hexylthiophene) derivatives, *J. Am. Chem. Soc.* 134 (2012) 5222–5232.
- [37] K.R. Graham, P. Erwin, D. Nordlund, K. Vandewal, R. Li, G.O.N. Ndjawa, E.T. Hoke, A. Salleo, M.E. Thompson, M.D. McGehee, A. Amassian, Re-evaluating the role of sterics and electronic coupling in determining the open-circuit voltage of organic solar cells, *Adv. Mater.* 25 (2013) 6076–6082.
- [38] N.K. Elumalai, A. Uddin, Open circuit voltage of organic solar cells: an in-depth review, *Energy Environ. Sci.* 9 (2016) 391–410.
- [39] H. Hoppe, M. Niggemann, C. Winder, J. Kraut, R. Hiesgen, A. Hinsch, D. Meissner, N.S. Sariciftci, Nanoscale morphology of conjugated polymer/fullerene-based bulk-heterojunction solar cells, *Adv. Funct. Mater.* 14 (2004) 1005–1011.
- [40] V.D. Mihailetschi, H.X. Xie, B. de Boer, L.J.A. Koster, P.W.M. Blom, Charge transport and photocurrent generation in poly(3-hexylthiophene): methanofullerene bulk-heterojunction solar cells, *Adv. Funct. Mater.* 16 (2006) 699–708.
- [41] A.J. Heeger, 25th Anniversary article: bulk heterojunction solar cells: understanding the mechanism of operation, *Adv. Mater.* 26 (2014) 10–27.